

1.70 Å X-Ray Structure of Human *apo* Kallikrein 1: Structural Changes Upon Peptide Inhibitor/Substrate Binding

Gurunathan Laxmikanthan,^{1,2} Sachiko I. Blaber,¹ Matthew J. Bennett,^{1,2} Isobel A. Scarisbrick,³ Maria Aparecida Juliano,⁴ and Michael Blaber^{1,2*}

¹*Institute of Molecular Biophysics Florida State University, Tallahassee, Florida*

²*Department of Chemistry and Biochemistry, Florida State University, Tallahassee, Florida*

³*Program for Molecular Neuroscience and Departments of Neurology, and Physical Medicine and Rehabilitation, Mayo Medical and Graduate Schools, Rochester, Minnesota*

⁴*Department of Biophysics, Universidade Federal de Sao Paulo, Escola Paulista de Medicina, Sao Paulo, Brazil*

ABSTRACT Human kallikreins are serine proteases that comprise a recently identified large and closely related 15-member family. The kallikreins include both regulatory- and degradative-type proteases, impacting a variety of physiological processes including regulation of blood pressure, neuronal health, and the inflammatory response. While the function of the majority of the kallikreins remains to be elucidated, two members are useful biomarkers for prostate cancer and several others are potentially useful biomarkers for breast cancer, Alzheimer's, and Parkinson's disease. Human tissue kallikrein (human K1) is the best functionally characterized member of this family, and is known to play an important role in blood pressure regulation. As part of this function, human K1 exhibits unique dual-substrate specificity in hydrolyzing low molecular weight kininogen between both Arg-Ser and Met-Lys sequences. We report the X-ray crystal structure of mature, active recombinant human *apo* K1 at 1.70 Å resolution. The active site exhibits structural features intermediate between that of *apo* and *pro* forms of known kallikrein structures. The S2 to S2' pockets demonstrate a variety of conformational changes in comparison to the porcine homolog of K1 in complex with peptide inhibitors, including the displacement of an extensive solvent network. These results indicate that the binding of a peptide substrate contributes to a structural rearrangement of the active-site Ser 195 resulting in a catalytically competent juxtaposition with the active-site His 57. The solvent networks within the S1 and S1' pockets suggest how the Arg-Ser and Met-Lys dual substrate specificity of human K1 is accommodated. *Proteins* 2005;58:802–814. © 2005 Wiley-Liss, Inc.

Key words: kallikrein; serine protease; substrate specificity; solvent structure; induced fit

INTRODUCTION

The kallikreins are a family of serine proteases that are distributed in a wide variety of tissues and biological

fluids. The term kallikrein is derived from the Greek word “kallikreas” which means pancreas, and historically this organ was the main source of these proteases.¹ It was believed for many years that the human kallikrein family had only three members; however, relatively recent studies have revealed that there are a total of 15 members that are co-localized at human chromosome loci 19q13.3-q13.4.^{2–4} Sequence analysis indicates the members of the human kallikrein family share 40–80% amino acid identity.⁴ The catalytic triad residues His57, Asp102, and Ser195 are conserved in each case, however, residue positions that define the different substrate-binding pockets exhibit heterogeneity. For example, position 189, located at the base of the S1 binding pocket, is observed to be either Asp, Gly, Glu, Ser, or Asn. Thus, the substrate P1 specificity of the kallikreins may vary considerably. Historically, rodents have been a focus for the study of the kallikreins. However, the rodent kallikrein gene locus appears to be uniquely different, and much more extensive, than the human. In addition to homologs of the 15 human kallikrein genes (i.e., KLK's), rodents exhibit approximately a dozen additional functional kallikrein genes known as “glandular” kallikreins (i.e., GK's).⁵

The human KLK family has gained attention in recent years due to the fact that most of the members appear to be differentially expressed in normal versus cancerous tissues, and this may prove to be a useful diagnostic in

Abbreviations: Ni-NTA, nickel-nitriloacetic acid; EK, enterokinase; SDS-PAGE, sodium dodecyl sulfate polyacrylamide gel electrophoresis; EDDnp, N-[2,4-dinitrophenyl]-ethylenediamine; TFA, trifluoroacetic acid; CAN, acetonitrile; MALDI-TOF, matrix assisted laser desorption ionization time-of-flight; EDTA, ethylenediamine tetraacetic acid; RMS, root mean square; BPTI, bovine pancreatic trypsin inhibitor.

The atomic coordinates and structure factors (code 1SPJ) have been deposited in the Protein Data Bank, Research Collaboratory for Structural Bioinformatics, Rutgers University, New Brunswick, NJ (<http://www.rcsb.org>).

*Correspondence to: Michael Blaber, 406 Kasha Laboratory, Institute of Molecular Biophysics, Florida State University, Tallahassee, FL 32306-3015. E-mail: blaber@sb.fsu.edu

Received 3 August 2004; Accepted 7 September 2004

Published online 13 January 2005 in Wiley InterScience (www.interscience.wiley.com). DOI: 10.1002/prot.20368

certain diseased states. For example, prostate-specific antigen (PSA, or "K3" —i.e., the protein product of the KLK3 gene) and K2 (the protein product of the KLK2 gene, confusingly also sometimes referred to as "glandular kallikrein" protein) are considered as the most useful biomarkers known for prostate cancer.^{6,7} Other kallikreins have been proposed as diagnostic markers for breast (K3, K6) and ovarian cancers (K6, K9, K10, and K11).^{8–12} More recently, several studies have shown that K6 may play a key role in the regulation of myelin turnover, and in demyelinating disease^{13–17} as well as the degradation of β -amyloid, or turnover of amyloid precursor protein.^{10,18} K8 has also been implicated in neuronal function (kindling epileptogenesis) in mice.^{19,20} Thus, the functional and biophysical properties of the kallikreins are of substantial current interest.

The most extensively studied member of the kallikrein family is "tissue kallikrein" or K1. This kallikrein is known to cleave various prohormones and bioactive peptides including kininogen, proinsulin, prorenin, and procollagenase²¹ and plays a major role in inflammation and heart disease. The prohormone kininogen is synthesized in the liver and is composed of two components: high molecular weight kininogen (120 kDa) and low molecular weight kininogen (68 kDa). Lysyl-bradykinin, or kallidin, is a decapeptide produced by the proteolytic action of K1 upon low molecular weight kininogen via cleavage between two specific bonds involving Met-Lys and Arg-Ser sequences, and this dual specificity of K1 is a unique functional property of this kallikrein.²² Lysyl-bradykinin is a vasoactive peptide that lowers blood pressure and plays an important role in blood pressure regulation.^{23–25} The actions of lysyl-bradykinin are opposed by angiotensin II, a vaso-constrictive peptide produced from the proteolytic cleavage of angiotensinogen I by angiotensin converting enzyme (ACE).^{26,27}

High-resolution structural information for the kallikreins, including stereochemical features of the catalytic residues, oxyanion binding pocket, and substrate binding pockets, will prove invaluable in drug design aimed at the development of specific substrates or inhibitors for this family of proteases. Unfortunately, structural data for the kallikrein family is limited; X-ray structures have been deposited for mouse *apo* K8 (PDB accession 1NPM),²⁰ porcine K1/inhibitor complexes with benzamidine (2PKA),²⁸ bovine pancreatic trypsin inhibitor (BPTI) (2KAI),²⁹ and hirustasin (1HIA),³⁰ and an apparently inactive form of horse K3 (1GVZ).³¹ Structures have also been deposited for mouse GK3 and GK4 in complex with nerve growth factor (1SGF),³² mouse *apo* GK13 (1AO5),³³ as well as Zn²⁺-inactivated rat GK2 (1TON).³⁴ As far as human kallikreins are concerned, only a single representative member (K6) is present in the Protein Data Bank: a 1.56-Å structure of human K6/benzamidine complex (1LO6)³⁵ and a 1.80 Å structure of a mutant form of *pro* human K6 (1GVL).³⁶ We report here the crystal structure determination of recombinant mature human *apo* K1 at 1.70 Å resolution. A comparison of this structure with the available kallikrein structures indicates that a variety of

structural changes occurs within the active site and substrate binding pockets of human K1 upon peptide inhibitor/substrate complex formation, and some of these structural changes appear necessary to form a catalytically competent active site.

MATERIALS AND METHODS

Cloning of Human KLK1, Expression and Purification of Human K1

The human KLK1 gene sequence information was obtained from Genbank (accession number AY094609). Two oligonucleotide primers useful for PCR amplification were synthesized based upon this information (KLK1-Fwd: 5'-ATT GTG GGA GGC TGG GAG TGT GAG C-3', and KLK1-Rev: 5'-TCA GGA GTT CTC CGC TAT GGT GTC C-3'; Integrated DNA technologies, Coralville IA). These primers were used to isolate full-length cDNA of the mature KLK1 from a human prostate cDNA library (Clontech, Palo Alto, CA) by PCR. The PCR product was subsequently cloned into the baculovirus transfer vector pBAC-3 (Novagen, Madison, WI) and transformed into competent *Escherichia coli* DH-5 α cells. Transformed colonies containing the appropriate insert were identified by screening with slot lysis electrophoresis in combination with restriction endonuclease digestion. The DNA sequence of the positive clones was confirmed using both forward and reverse sequencing, and was in agreement with accession number A Y094609.

A baculovirus/insect cell line (Novagen, Madison, WI) was used as the expression host to produce recombinant protein as previously described.³⁵ Briefly, the expression construct utilizes an amino-terminal gp64 virus secretion signal, a six-residue His tag, and enterokinase (EK) recognition sequence, respectively, fused to the amino terminal of the mature K1 sequence. Infection of the insect cell line and production of the secreted recombinant protein was performed as previously described.³⁵ The media containing the secreted K1 protein was harvested by centrifugation at 5,000 \times g, followed by 0.2 μ m filtration of the supernatant, and then loaded directly onto nickel-nitriloacetic acid (Ni-NTA) resin (QIAGEN Inc., Valencia, CA). Elution of the nickel-affinity resin was performed using a step gradient of 250 mM imidazole in 50 mM Tris HCl, 150 mM NaCl, 0.01 % Tween, pH 7.5. The eluted K1 fractions were pooled and dialyzed against 40 mM sodium acetate, pH 4.5 using 6–8-kDa molecular weight cutoff dialysis tubing (Spectrum Laboratories, Rancho Dominguez, CA). All purification steps were performed at 4°C.

Activation of Recombinant Human K1

As mentioned above, the expression construct substitutes the EK pro-sequence for the natural human K1 pro-sequence. Thus, activation was accomplished by the addition of EK to yield a 1:200 EK:K1 molar ratio, followed by incubation at 37°C for 150 min. These conditions yielded essentially complete digestion of the EK pro-sequence (monitored using SDS-PAGE) and release of mature K1 protein. The mature K1 protein was immediately loaded onto a 2.5 \times 100-cm Sephadex G-50 (Pharma-

TABLE I. Structural Regions Utilized in an Overlay of the Human *apo* K1 Structure With Available Kallikrein Structures[†]

Protein	PDB	Structurally conserved regions	RMS (Å)
Human <i>pro</i> -K6	1GVL	24–73, 82–94, 98–128, 134–141, 153–171, 175–185, 188, 194–216 and 223–244	1.09
Human K6/benzamidine complex	1LO6	16–35, 38–94, 98–128, 134–145, 147–171, 175–184, 187–220, 223–243	1.08
Porcine K1/benzamidine complex	2PKA	16–24, 26–95, 97–147, 148–246	0.81
Porcine K1/bovine pancreatic trypsin inhibitor (BPTI) complex	2KAI	16–95, 97–147, 148–170, 174–245	0.88
Porcine K1/hirustasin complex	1HIA	16–95, 97–147, 148–245	0.83
Horse K3	1GVZ	16–35, 38–95, 98–142, 153–170, 172, 175–184, 187, 190–191, 194–214, 224, 227–246	1.07
Mouse <i>apo</i> K8	1NPM	16–35, 39–75, 79–95, 98–114, 116–172, 175–185, 187–221, 223–243	0.88
Mouse GK3/nerve growth factor complex	1SGF	16–35, 38–95, 97–245	0.74
Mouse <i>apo</i> GK13	1AO5	16–35, 38–95, 97–146, 149–246	0.66
Rat GK2/zinc complex	1TON	16–35, 41–95, 99–169, 176–177, 179–214, 219–246	0.82

[†]RMS deviations for main-chain atoms for the overlay are provided.

cia Corp., Kalamazoo MI) gel-filtration column and eluted with a running buffer of 40 mM sodium acetate, 100 mM NaCl at pH 4.5. The eluted fractions were pooled for subsequent use in crystallization trials.

Crystallization and Data Collection of Mature Recombinant Human K1

The molar extinction coefficient of mature human K1 was calculated to be $51,832 \text{ M}^{-1} \text{ cm}^{-1}$ (280 nm) based on the spectroscopic method of Gill and Von Hippel.³⁷ The purified K1 protein was concentrated to 10 mg/ml and crystallization trials were performed using the hanging drop vapor diffusion method and a sparse matrix screen of precipitants, salts, and buffers.³⁸ Rod-shaped diffraction quality crystals grew from 24% polyethylene glycol 3350, 100 mM Tris 6.5, 150 mM calcium acetate after 8 weeks incubation at 4°C. Crystals were briefly transferred to a cryo-protectant solution consisting of mother liquor and 20% glycerol prior to freezing under a stream of nitrogen gas at 103 K. Diffraction data were collected at 103 K from a single crystal ($0.7 \times 0.3 \times 0.06 \text{ mm}$) using a MARCCD 165 detector (MAR-USA, Inc., Evanston IL) in combination with a Rigaku RU-H2R rotating anode X-ray source equipped with an Osmic Blue confocal mirror system (Mar USA Inc., Evanston IL). Diffraction data were indexed, integrated and scaled using the DENZO and SCALEPACK software packages.^{39,40}

Structure Refinement of Mature Recombinant Human K1

The entire structure of mature human K6 (PDB accession code 1LO6),³⁵ sans solvent, was used as a search model in the molecular replacement technique to obtain initial phase information. Rotation and translation function searches were performed using the CNS software package.⁴¹ After an initial solution was found, 5% of the data in the reflection file was set aside for R_{free} calculations.⁴² Manual model building and visualization of the structure was performed using the O software package,⁴³

and refinement by simulated annealing, using a maximum likelihood target, was performed using the CNS software package.⁴¹ Side chains that differed between the K6 search model and K1 sequence were deleted and subsequently rebuilt into $2F_o - F_c$ composite omit maps, and rotamer orientations for side chains positions that are shared between the K6 search model and K1 were similarly confirmed or adjusted. Insertions in the K1 structure relative to the K6 search model were built into $2F_o - F_c$ composite omit maps. Solvent molecules were added at the end of the refinement and manually checked for appropriate stereochemistry, $2F_o - F_c$ difference electron density, and refined thermal factors.

Structural Alignments with Available Kallikrein Structures

Structural alignment of the refined human K1 structure with available kallikrein structures was performed using the Swiss PDB Viewer (SPDBV) software.⁴⁴ The structurally-conserved regions utilized in such overlays, and the associated root-mean-square deviations (RMS) for main-chain atoms, are listed in Table I.

Naturally Isolated Human K1 Protein

Homogeneous preparations of human K1, obtained according to Shimamoto et al.⁴⁵ were kindly provided by Dr. J. Chao of the Medical University of South Carolina, SC, Charleston, USA. The molar concentrations of enzyme solutions were determined by active site titration with 4-methyl-umbelliferyl-p-guanidinobenzoate using a previously described procedure.⁴⁶

Preparation of Synthetic Substrates

Intramolecularly quenched fluorogenic peptides containing N-[2,4-dinitrophenyl]-ethylenediamine (EDDnp) attached to glutamine (a necessary result of the solid-phase peptide synthesis strategy employed) were synthesized as previously described.⁴⁷ The final deprotected peptides were purified by semi preparative HPLC using an Econosil

TABLE II. Kinetic Parameters for Hydrolysis of Peptides Derived From the Sequence Abz-KLXSSKQ-EDDnp by Naturally Derived and Recombinant Human K1[†]

X	Naturally derived human K1			Recombinant K1		
	k_{cat} s ⁻¹	K_m μ M	k_{cat}/K_m (mM s) ⁻¹	k_{cat} s ⁻¹	K_m μ M	k_{cat}/K_m (mM s) ⁻¹
R	3.7	1.0	3700	3.7	1.5	2467
K	0.9	1.2	714	1.4	2.7	519
F	0.3	2.2	155	0.9	3.9	231

[†]The X represents the P1 position in the substrate, with hydrolysis occurring at the X-S bond.

C-18 column (10 μ m, 22.5 \times 250 mm; Alltech Associates, Inc., Deerfield IL) and a two-solvent system: (A) trifluoroacetic acid (TFA)/H₂O (1:1000) and (B) TFA/acetonitrile (CAN)/H₂O (1:900:100). The column was eluted at a flow rate of 5 ml/min with a 10 (or 30) – 50 (or 60)% gradient of solvent B over 30 or 45 min. Analytical HPLC was performed using a binary HPLC system from Shimadzu with a SPD-10AV Shimadzu uv-vis detector and a Shimadzu RF-535 fluorescence detector, coupled to an Ultrasphere C-18 column (5 μ , 4.6 \times 150 mm; SGE Incorporated, Austin, TX) eluted with solvent systems A1 (H₃PO₄/H₂O, 1:1000) and B1 (CAN/ H₂O/H₃PO₄, 900:100:1) at a flow rate of 1.7 ml/min and a 10–80% gradient of B1 over 15 min. The HPLC column eluates were monitored by their absorbance at 220 nm and by fluorescence emission at 420 nm following excitation at 320 nm. The molecular weight and purity of synthesized peptides were checked by ToF-Spec-E MALDI-TOF mass spectrometry (Waters Corporation, Milford, MA) and peptide sequencing using a Shimadzu PPSQ-23 protein sequencer. HPLC analysis of the different fluorogenic substrates did not show any significant contamination, and their concentration in solution could be determined from the fluorescence obtained following total tryptic hydrolysis and by colorimetric determination of 2,4-dinitrophenyl group ($E_{365nm} = 17,300 \text{ M}^{-1}\text{cm}^{-1}$).

Fluorometric Enzyme Assay

The hydrolysis of the fluorogenic peptide substrates was followed by measuring the fluorescence at $\lambda_{ex} = 320$ nm and $\lambda_{em} = 420$ nm in a Hitachi F-2000 spectrofluorometer (Hitachi High Technologies America, Inc., San Jose, CA) at 37°C in 20 mM Tris-HCl, pH 9.0 containing 1 mM EDTA. A 1-cm path-length cuvette containing 2 ml of the substrate solution was placed in the temperature controlled holder for 5 min before the enzyme solution was added. Upon addition of enzyme, the increase in fluorescence signal was continuously recorded for 10 min. The enzyme concentrations for initial rate determinations were chosen so as to hydrolyze less than 5% of the substrate present. The kinetic parameters were calculated according to Wilkinson⁴⁸ as well as by analysis of Eadie-Hofstee plots. The standard errors for K_m and k_{cat} determinations were less than 5% in each case. The cleavage site for each substrate was determined by isolation of the substrate(s) and mass determination by a ToFSpec-E MALDI-TOF mass spectrometer.

RESULTS

Purified Recombinant Human K1

The purified recombinant mature human K1 exhibited a single band of ~30 kDa on SDS PAGE under reducing conditions, suggesting a single-chain form with no internal cleavages. Under nonreducing conditions the protein migrated as a single band but exhibited a slightly lower apparent molecular mass, indicating a more compact state due to the five disulfide bonds within the structure. The purity was estimated at better than 95% based upon the Coomassie blue staining of the SDS PAGE. The MALDI-TOF mass spectra showed an average mass of 28,780 Daltons, but as a cluster of peaks separated by approximately 180 Da (data not shown), suggesting the presence of heterogeneity in the glycosylation of the protein. Amino terminal sequence analysis indicated the presence of a single sequence, with no detectable minor sequence, in agreement with the expected mature human K1 amino terminus. Naturally isolated human K1 and the purified recombinant K1 hydrolyzed the tested substrates with similar kinetic parameters (Table II).

X-Ray Data Collection and Structure Refinement

Crystals of recombinant K1 diffracted to better than 1.70 Å, and maintained high resolution diffraction after prolonged X-ray exposure, permitting a substantially complete data set to be collected using a single crystal (Table III). Indexing of the reflections suggested an orthorhombic space group with cell dimensions of $a = 44.7$ Å, $b = 76.4$ Å, $c = 76.6$ Å. The Matthews' coefficient had a value of 2.27 Å³/Da with space group P2₁2₁2₁ and one molecule in the asymmetric unit, suggesting that a single molecule represented the contents of the asymmetric unit.⁴⁹ A rotation function search using the human K6 structure (1LO6), sans solvent, yielded a single peak of 5 σ , and a translation search of this solution using the P2₁2₁2₁ space group produced a single peak of 3 σ . A subsequent rigid body refinement of the rotated and translated search model resulted in a value for R_{crist} of 42.4%, indicating that the space group had been correctly assigned, the search model had been correctly positioned to provide initial phase information, and that there was indeed a single molecule in the asymmetric unit. An initial $2F_o - F_c$ composite omit map confirmed the general correctness of the molecular replacement solution.

TABLE III. Crystal, Data Collection, and Refinement Statistics for the Human apo K1 Structure

Crystal data	
Space group	P2 ₁ 2 ₁ 2 ₁
Cell dimensions (Å)	a = 44.7 Å, b = 76.4 Å, c = 76.6 Å
Molecules/asymmetric unit	1
Matthews' coefficient (V _m) Å ³ /Da	2.27
Resolution range (Å)	50–1.70
Data collection and processing	
Total/unique reflections	138, 151/27, 963
Completion (50–1.70 Å)/(1.73–1.70 Å) (%)	94.3/89.2
I/σ (50–1.70 Å)/(1.73–1.70 Å)	37.6/5.9
R _{merge} (%) (50–1.70 Å)/(1.73–1.70 Å) ^a	6.1/38.5
Wilson temperature factor (Å ²)	13.4
Refinement	
R _{cryst} (50–1.70 Å) ^b	17.2
R _{free} (50–1.70 Å) ^b	20.2
RMS bond length deviation (Å)	0.009
RMS bond angle deviation (°)	1.6
Ramachandran plot	
Most favored region	89.0
Additionally allowed region	10.5
Generously allowed region	0.5
Disallowed region	0.0
Number of atoms/molecule	
Non-H protein	1837
Water/ion	358/2

^aR_{merge} = $\sum |I_i - \langle I \rangle| / \sum I_i$, where I_i is the intensity of the i th observation and $\langle I \rangle$ is the mean intensity of the reflection.

^bR = $\sum ||F_o| - |F_c|| / \sum |F_o|$, where F_o and F_c are the observed and calculated structure factor amplitudes.

The human K1 protein comprises 237 residues, whereas, the human K6 model comprises 222. There are three locations within the structure of human K1 where there are insertions relative to the K6 search model, including an 11-amino-acid insertion after position 94 (i.e., the “kallikrein loop”), a two-amino-acid insertion after position 144, and a two-amino-acid insertion at the C-terminus (numbering scheme of chymotrypsinogen). Furthermore, the human K1 and K6 proteins share amino acid identity at 89 positions, therefore, the model building of human K1 involved the substitution of 133 amino acids in addition to the insertion of the 15 amino acids described above.

A $2F_o - F_c$ difference electron density was visible for the entire polypeptide chain of the K1 model, with the exception of residue positions 95G and 95H, located within the “kallikrein loop.” SDS PAGE analysis of a K1 crystal grown from the same mother liquor and for an identical length of time did not show any evidence of proteolytic degradation. Thus, we conclude that the lack of density for the 95G and 95H residues is due to positional disorder in this region of the kallikrein loop. The side chains of some surface residues exhibited discontinuous electron density and these atoms were given zero occupancy. Alternate conformations were modeled for the side chains of residues 195 and 230. The electron density suggested the presence of two calcium ions in the structure. The first calcium ion coordinates with Lys 169, His 172, and Asp 75 (where the latter belongs to a symmetry-related molecule). This cal-

cium ion displays an extensive coordination of water molecules forming a pentagonal bipyramidal network. The second calcium ion hydrogen bonds to Asn 245 and displays a similar coordination of local solvent molecules, and with no symmetry-related contacts.

Porcine K1 contains a glycosylation site at position Asn 95²⁹ and human K1 contains the same potential glycosylation site. The $2F_o - F_c$ difference electron density of K1 indicated well-defined density for an N-acetyl glucosamine sugar moiety adjacent to the side chain of Asn 95. No electron density was present to indicate ordered positions for additional carbohydrate moieties beyond this initial N-acetyl glucosamine, and the general orientation of the polysaccharide was toward solvent space within the crystal.

The active site Ser 195 in the human K6 search model (1LO6) exhibits the characteristic *gauche+* side chain χ_1 angle ($\sim -60^\circ$) which positions the side chain O γ within hydrogen bonding distance (2.67 Å) of the neighboring active site His 57 N ϵ^2 atom. However, in this orientation the $F_o - F_c$ difference electron density exhibited a well-defined region of electron density adjacent to the Ser 195 C β , indicating the presence of a *gauche-* rotamer ($\chi_1 \sim +60^\circ$) for this side chain. Modeling this alternate orientation resulted in similar difference density indicating the presence of a *gauche+* rotamer (Fig. 1). Thus, the side chain of Ser 195 was modeled in both the *gauche+* and *gauche-* rotamers with half occupancy for each. The O γ of the *gauche-* rotamer exhibited a refined thermal factor value of 8 Å² while the *gauche+* rotamer had a value of 18 Å². Thus, while the *gauche+* rotamer is the expected conformation for an active site Ser, the *gauche-* rotamer appears to be more substantially defined in the electron density map. No inhibitors were added to the crystallization buffer, and no unusual electron density was observed within the active site. Thus, the refined K1 structure represents the mature *apo* form of human K1.

DISCUSSION

Historically, the first kallikrein structure solved was a 2.0 Å structure of naturally isolated porcine K1, in complex with benzamidine inhibitor, reported by Bode and coworkers in 1983.²⁸ In addition to the previously mentioned mouse K8, horse K3, and rodent mGK structures, the intervening years have seen the deposition of only two structures for the human kallikreins, both involving K6 (i.e., mature K6/benzamidine complex [1LO6] and a mutant *pro* K6 [1GVL]). Katz and coworkers⁵⁰ reported a 2.0-Å X-ray structure determination of a quadruple mutant form (Gln24→Arg/Asp95→Asn/Asp98C→Asn/Asp148→Asn) of human *apo* K1 designed to eliminate sites of potential glycosylation. This was a challenging structural determination since the crystals were reported to be X-ray sensitive and only partial data sets could be collected for a given individual crystal. Furthermore, although the crystals diffracted to 1.64 Å, acceptable merging statistics could only be accomplished by limiting the merging resolution to 2.0 Å, and it was necessary to combine a total of five crystal data sets to produce an appropriately complete data set. Despite this achieve-

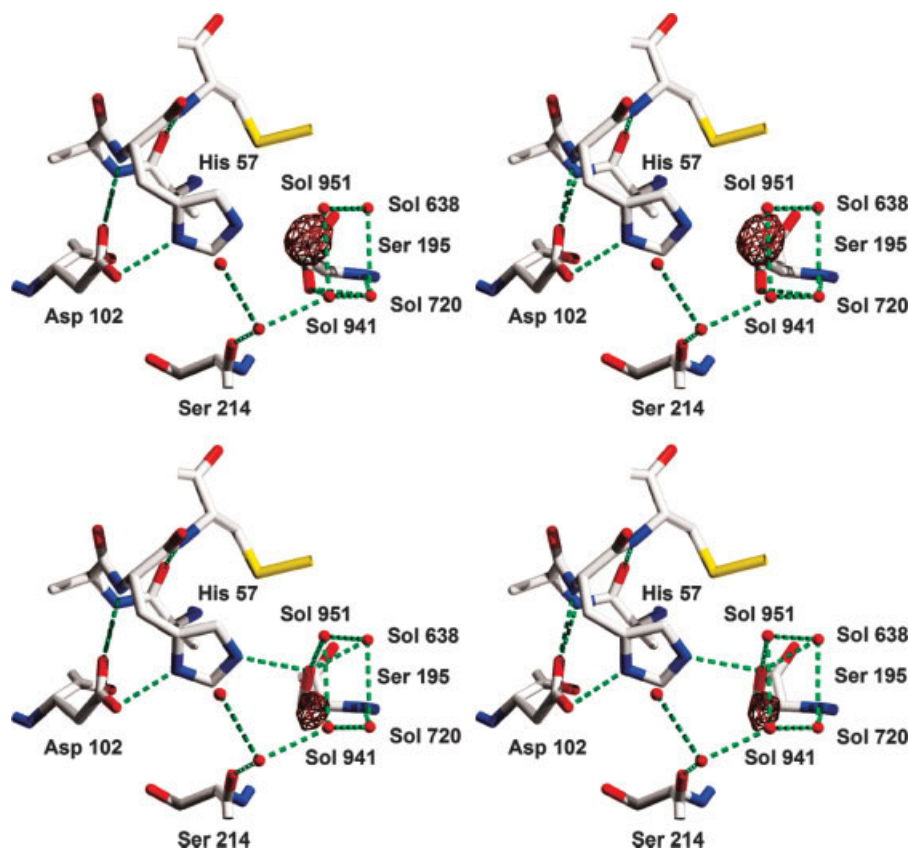


Fig. 1. **Top:** relaxed stereo diagram of the active site region of the human *apo* K1 structure with the catalytic Ser 195 modeled in the *gauche+* rotamer. Overlaid onto the structure is the F_o-F_c difference density map contoured at 4σ . Difference density adjacent to the Ser 195 O^γ indicates the presence of an alternative *gauche-* rotamer. **Bottom:** an identical view but with the active site Ser 195 refined in the *gauche-* rotamer. Overlaid onto the structure is the F_o-F_c difference density map contoured at 4σ . Difference density adjacent to the Ser 195 O^γ indicates the presence of the alternative *gauche+* rotamer. Also shown in each panel are the hydrogen-bonding networks in the vicinity of Ser 195.

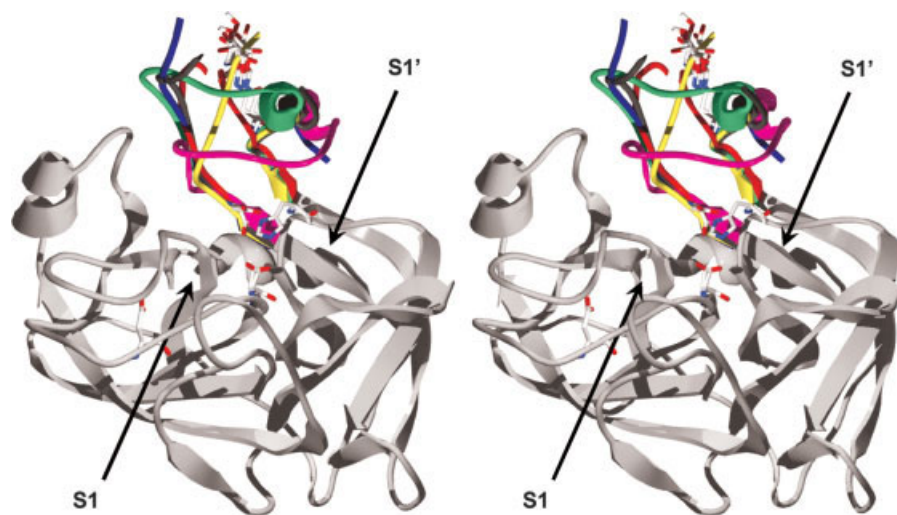


Fig. 2. Relaxed stereo diagram ribbon drawing of the human *apo* K1 structure (light grey) and the overlaid kallikrein loop regions of horse K3 (1GVZ, magenta), porcine K1 (2PKA, red), mouse GK3 (1SGF, blue), mouse GK13 (1AO5, green) and rat GK2 (1TON, yellow), with the human K1 kallikrein loop indicated in dark grey. The active site His 57, Asp 102, and Ser 195 residues in human K1, as well as the Asp 189 at the base of the S1 pocket are indicated in wire frame representation. The location of the S1 and S1' pockets are indicated. The carbohydrate moiety attached to Asn 95, observed in the human K1, mouse GK3 and mouse GK13 structures, is also indicated in wire frame shown.

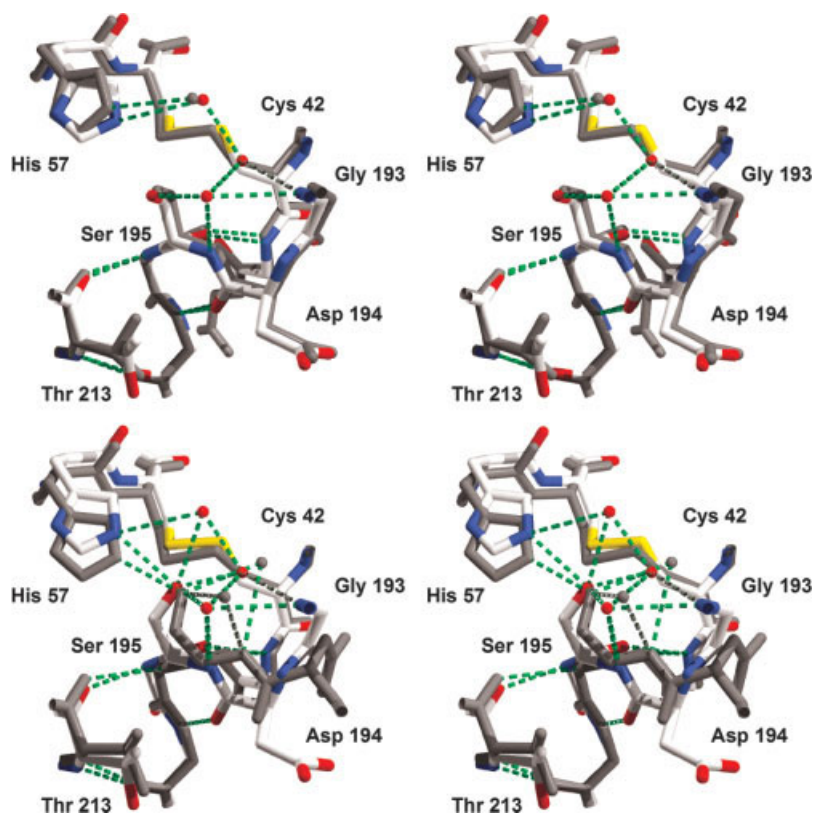


Fig. 3. **Top:** relaxed stereo diagram of the active site of human *apo* K1, with the active site Ser 195 *gauche*⁺ rotamer shown, overlaid with the active site in mouse *apo* K8 (1NPM; grey). **Bottom:** relaxed stereo diagram of the active site of human *apo* K1, with the active site Ser 195 *gauche*⁻ rotamer shown, overlaid with the active site of *pro* human K6 (1GVL; grey).

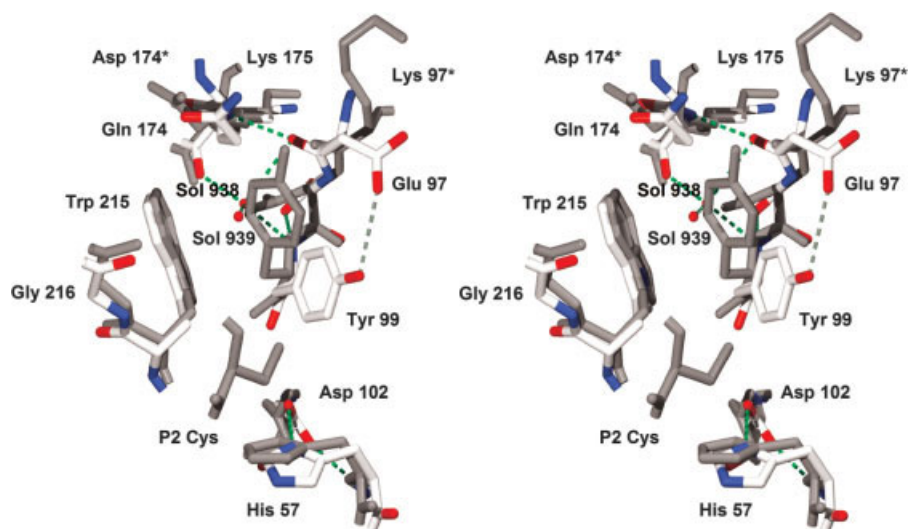


Fig. 4. Relaxed stereo diagram of the S2 pocket in human *apo* K1 (CPK coloring) overlaid with porcine K1/BPTI complex (2KAI; grey). The location of the P2 Cys residue in the BPTI is shown. Formation of the hydrophobic S2 pocket is likely to involve a conformational change of Tyr 99 and the concomitant displacement of solvent molecule 939. The locations of the active site His 57 and Asp 102 are also shown.

ment, the coordinates were never deposited. In the present study we report a high-resolution (1.70-Å) X-ray structure of nonmutagenized human K1, from a single crystal, and with excellent statistics of completion, redundancy and

signal-to-noise. Although Katz and coworkers did not provide details of their space group, two molecules were present in their asymmetric unit, and it therefore differs from the crystal form reported here.

The Kallikrein Loop

The human K6 structure, utilized as the molecular replacement search model, does not contain the extended “kallikrein loop” after residue position 95 that is present in human K1 and some other members of the kallikrein family. In human K1 this loop contains an 11-amino-acid insertion (residue positions 95A–95K) between residues 95 and 96 (using the classical chymotrypsinogen numbering scheme). Available kallikrein structures that contain a loop of identical length (albeit with different amino acid sequence) include porcine K1, horse K3, mouse GK3, mouse GK13, and rat GK2. An overlay of the human *apo* K1 structure with these other kallikreins, and highlighting the kallikrein loop regions, is shown in Figure 2.

The structures of human K1, horse K3, and mouse GK13 all display a characteristic helical turn within residue positions 95B–95D of the kallikrein loop. In a comparison of the aligned human K1 and horse K3 structures, the kallikrein loops (i.e., residue positions 92–95F and 95K–99) overlay with a root-mean-square deviation (RMSD) of 3.5 Å. However, the main-chain atoms of residue positions 92–95F alone from both structures overlay with a RMSD of 0.6 Å and the main-chain atoms of residue positions 95K–99 alone overlay with a RMSD of 1.0 Å. The two groups of atoms together, and separate from the rest of the molecule, overlay with a RMSD of 1.4 Å. Thus, the kallikrein loops in the human K1 and horse K3 structures can be characterized as being structurally similar, but exhibiting a generalized “hinge-bending” motion in the region of positions 91 and 100. The kallikrein loop structure of mouse GK13 (1AO5) is observed to be essentially identical to that of human K1, and similar also to the observable region of the mouse GK3 (1SGF) kallikrein loop. This similarity extends to the conformation of the carbohydrate moiety attached to residue Asn 95, which is essentially juxtaposed when comparing each of these structures (Fig. 2). In contrast, the human K1 kallikrein loop structure is considerably different from that observed in the porcine K1 (2PKA) or rat mGK2 (1TON) structures. In these two structures the kallikrein loop exhibits a generalized hinge-bending motion that orients these loops in the opposite direction from the active site. The range of conformations observed for the kallikrein loop in these structures may reflect dynamic hinge-bending motions that are available to this loop. Indeed, the array of conformations observed is strikingly similar to the conformational variability predicted from molecular dynamics simulations of a model of human K3.⁵¹ The juxtaposition of the kallikrein loop to the active site suggests that this loop may affect substrate access to the active site. In this regard, the horse K3 is the most “closed” and the porcine K1 the most “open” conformation. The horse K3 structure has been proposed to represent an enzymatically inactive structure, in part due to the “closed” conformation of the kallikrein loop.³¹ We propose that the close similarity of the loop conformation, including carbohydrate moiety, for the human K1, mouse GK3, and mouse GK13 structures, despite different amino acid sequences, space groups, and

packing interactions, suggests that this conformation likely represents a low-energy structure for the kallikrein loop.

Active-Site Ser 195

The two different conformations observed for the active-site Ser 195 represent either the time-averaged structure within the unit cell, or the average of distinctly different conformations present within the different unit cells comprising the crystal lattice. In either orientation the Ser 195 conformation is not in a catalytically functional juxtaposition with the other residues of the catalytic triad, in particular, His 57. The orientation of the active site Ser in the human K6 search model follows the characteristic orientation for the chymotrypsin type serine proteases: a *gauche+* rotamer ($\chi^1 \sim -60^\circ$) with the Ser O γ within hydrogen-bonding distance (2.67 Å in the case of ILO6) to the active site His 57 N ϵ^2 , and positioned to undertake a nucleophilic attack upon the carbonyl carbon of the P1 substrate residue.^{29,52–56} However, in the refined human *apo* K1 structure, the Ser 195 in the *gauche+* rotamer moves ~ 0.7 Å away from the His 57 side chain, increasing the His 57 N ϵ^2 –Ser 195 O γ distance to more than 3.4 Å, and reducing the Ser C β –O γ –His 57 N ϵ^2 angle to less than 70° (Fig. 3). Solvent, and not the His 57 side chain, is observed to be the hydrogen-bonding partner of Ser 195 in this orientation, thus, the serine hydroxyl is unlikely to be an activated nucleophile.⁵⁷ In contrast, the *gauche-* rotamer positions the Ser 195 O γ 2.86 Å from the His 57 N ϵ^2 atom, and with a C β –O γ –N ϵ^2 hydrogen-bonding angle of 97°. Thus, the His N ϵ^2 atom is the hydrogen-bonding partner for the Ser 195 in this alternative orientation, however, the Ser is now incorrectly positioned for a nucleophilic attack upon a the P1 carbonyl carbon of a bound peptide substrate.

Although different from the human K6 search model, the structural details of the *gauche+* Ser 195 rotamer are strikingly similar to the mouse K8 structure (1NPM), including aspects of the local solvent structure (Fig. 3, top). The mouse K8 structure is also an *apo* form, although alternative conformations were not reported for the Ser 195 in this structure.²⁰ The *gauche-* rotamer for the Ser 195 has not previously been reported for an active member of the chymotrypsin type serine proteases, but is observed in the structure of *pro* human K6 (1GVL).³⁶ The local details of the Ser 195 in the *gauche-* rotamer, including solvent structure, are strikingly similar between the human *apo* K1 and inactive *pro* K6 structures (Fig. 3, bottom). The lack of enzymatic activity for the *pro* form of human K6 has been attributed, in part, to the structural details that result in this orientation of the active site Ser.³⁶ The enzymatic characterization of the recombinant human K1 protein, however, indicates that it is just as active, upon addition of substrate, as the naturally-derived enzyme (Table II). An overlay of the human *apo* K1 crystal structure with either the porcine K1/BPTI or hirustasin complexes indicates that a residue bound in the S1 pocket would result in a close ~ 2.0 Å contact distance between the P1 main chain C α and the Ser 195 side chain O γ for the Ser 195 *gauche+* rotamer in the K1 structure. Furthermore,

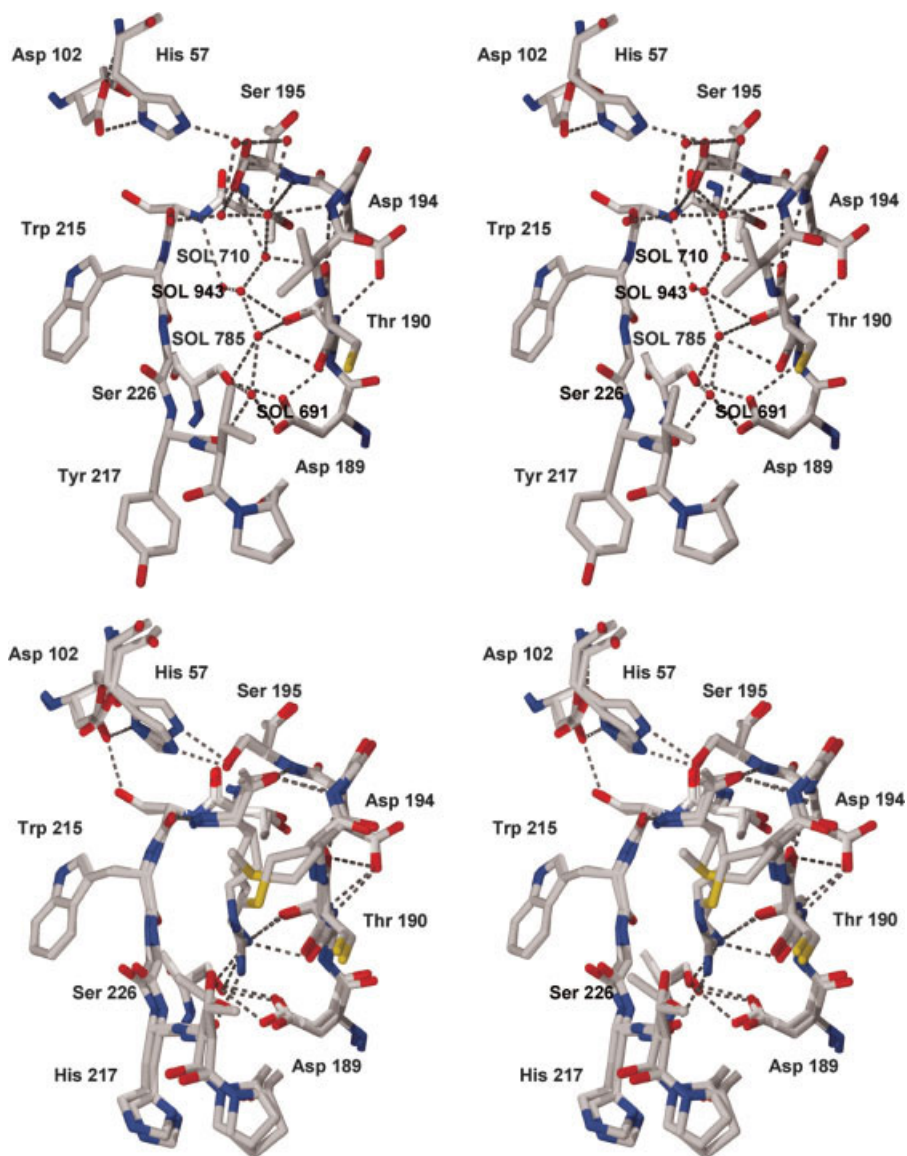


Figure 5.

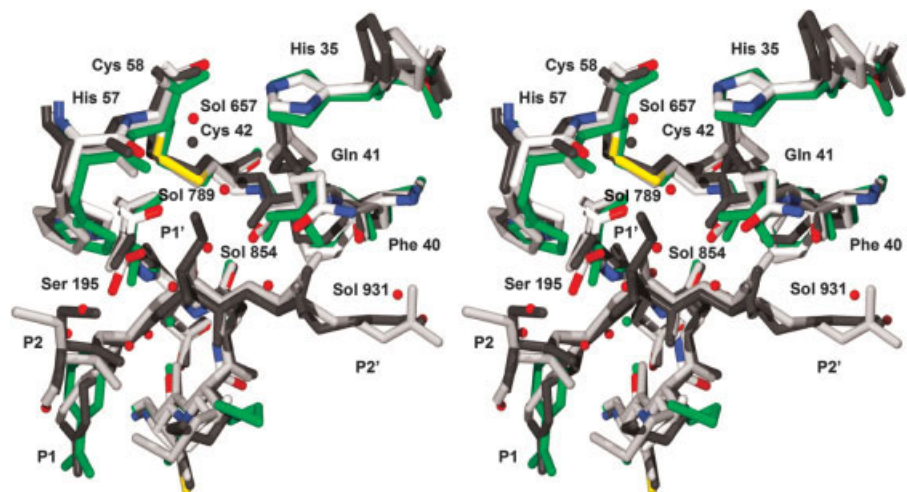


Figure 6.

for the *gauche*- rotamer there would be similarly close contact distances between the bound P1 main-chain carbonyl carbon and the Ser 195 C β (~ 2.6 Å) and Ser 195 O γ (~ 2.3 Å). These structural comparisons indicate that the binding of a P1 residue in the S1 pocket serves to position the human K1 active site Ser 195 to a catalytically competent orientation (i.e., *gauche*+ rotamer, and ~ 2.8 Å hydrogen bonding interaction with the catalytic His 57 N ϵ^2 atom).

S2 Pocket

Approximately 80% of the binding energy of peptide substrates and inhibitors to human K1 is contributed by interactions within the S2 to S1' pockets.⁵⁸ Furthermore, interactions within the S2 to S2' pockets are primary determinants of Met-Lys bond cleavage specificity, and interactions within the S1' to S3' pockets have been identified as important contributors to efficient hydrolysis of short peptide substrates.⁵⁹ These, and other studies, identify interactions within the S2 to S2' pockets as forming essential structural determinants of substrate specificity and catalytic efficiency for human K1.

The S2 pocket of both human and porcine K1 comprises a hydrophobic cleft formed by the side chains of residues Trp 215 and Tyr 99.²⁹ This hydrophobic cleft has been proposed to form the basis of the preference of human and porcine K1 for substrates with hydrophobic P2 residues.^{29,58,59} While the Trp 215 side chain exhibits a characteristically conserved rotamer orientation in all K1 structures (porcine K1/benzamidine complex (2PKA); porcine K1/BPTI complex (2KAI); porcine K1/hirustasin complex (1HIA); and the present report), the Tyr 99 side chain exhibits a variety of conformations in the different K1 structures. In the porcine K1 complex with benzamidine in the S1 pocket (but with no moiety within the S2 pocket) (2PKA) the Tyr 99 side chain adopts a χ angle of -119° and χ_2 of 99° ,²⁸ however, this side chain exhibits an average B factor of 61.3 Å² indicating that it is poorly defined in the structure. In contrast, when complexed with BPTI (2KAI), which contains a Cys residue at the inhibitor P2 position, the Tyr 99 side chain adopts a χ_1 angle of -39° and χ_2 of 97° . Furthermore, in contrast with the 2PKA structure, the average B factor for the Tyr 99 side chain is 8 Å²,²⁹ indicating that the Tyr 99 side chain has become highly ordered in the presence of a bound P2 side chain. The P2 Cys in the porcine K1/hirustasin complex (1HIA), adopts a

χ_1 angle of -56° and a χ_2 angle of -41° , with average B factors of 43 Å², but does not actually orient towards the S2 pocket.³⁰ Despite the structural variations described above, a common feature of the Tyr 99 and Trp 215 interaction for all porcine K1 structures is the presence of *van der Waals* contacts between the two residues. In the human *apo* K1 structure, the side chain of Tyr 99 exhibits well-defined electron density, with a χ_1 of -78° and χ_2 of 62° and average refined B factors of 33.9 ± 5.4 Å². However, the cleft between Trp 215 and Tyr 99 in human *apo* K1 is broader by approximately 0.7 Å in comparison to the porcine K1 structures. In addition to being broader, the human *apo* K1 structure exhibits a clearly defined intervening solvent molecule (Sol 939, B factor of 27.7 Å², Fig. 4) between these side chains. This solvent is positioned centrally with regard to the aromatic ring of the side chain Trp 215 and at a distance of 3.2 Å normal to the center of this ring, and is therefore optimally positioned to hydrogen-bond with the π electron cloud of the aromatic ring of Trp 215. This hydrated open form of the S2 pocket has not previously been described for any kallikrein structure. A comparison of the human *apo* K1 and inhibited porcine K1 structures suggests that this solvent is excluded, and the Trp 215 and Tyr 99 residues move closer to each other, forming the characteristic hydrophobic S2 pocket geometry, upon substrate binding.

S1 Pocket

The S1 pocket is formed by the main-chain atoms of residue positions 214–217 and 189–195, and includes interactions by the side chains of positions 189, 190, 195, 216, and 226, which are identical between human and porcine K1. The S1 pocket of the human *apo* K1 structure contains a string of solvent molecules (solvent 710, 943, 785, and 691, respectively), that extend from the proximity of Ser 195 to Asp 189. These solvent molecules form a contiguous hydrogen-bonding network, with solvent 691 residing at the “bottom” of the S1 pocket and hydrogen bonding to Asp 189 (Fig. 5). These solvents are well-defined, with B factors of 24.8 Å² (710), 33.8 Å² (943), 35.2 Å² (785), and 18.6 Å² (691). A comparison of the human *apo* K1 structure with the various porcine K1 structures indicates that solvents 710 and 943 are displaced by the hydrophobic side chain C β , C γ , and C δ atoms of the P1 side chain Arg (1HIA) or Lys (2KAI) residues. A similar comparison of the structure of bovine β -trypsin in complex with a mutant form of BPTI containing a Met at the P1 positions (3BTM⁶⁰), also indicates that solvent 710 and 943 (but neither 785 nor 691) would be displaced by this side chain. The Met χ_3 angle in 3BTM adopts a different conformation in comparison to the P1 Lys or Arg side chains in 1HIA and 2KAI, and positions the C ϵ of the Met towards the side of the pocket, thus, solvent 785 would not be displaced and the 3BTM structure contains a solvent (653) that is equivalent to that of 785 in human *apo* K1. Neither solvent molecule 710 or 943 is an exclusive hydrogen bonding partner for any protein atom, thus their displacement by a hydrophobic side chain carbon atom does not result in an unsatisfied hydrogen bonding partner within the S1 pocket.

Fig. 5. **Top:** relaxed stereo diagram of the S1 pocket of human *apo* K1 and the solvent network occupying this pocket. **Bottom:** relaxed stereo diagram of porcine K1 in complex with BPTI (2KAI); with Lys in the S1 pocket) and hirustasin (1HIA; with Arg in the S1 pocket), and shown in the same orientation as human *apo* K1 in the top panel. The solvent molecules in the S1 pocket of human *apo* K1 are displaced by approximately equivalent atomic positions of the P1 Arg and Lys side chains (see text).

Fig. 6. Relaxed stereo diagram of the S1' pocket of human *apo* K1 overlaid with the structures of porcine K1/benzamidine complex (2PKA; green), porcine K1/BPTI complex (2KAI; light grey and with Ala in the P1' position), and porcine K1/hirustasin complex (1HIA; dark grey and with Ile in the P1' position). Concerted positional alterations are observed for Gln 41 and His 35 upon binding of a P2' main-chain group.

Solvent 785 is replaced by Lys N^ε (2KAI) or Arg N^{η1} (1HIA) and solvent 691 is replaced by Arg N^{η2} (1HIA). Solvent 785 serves as the exclusive hydrogen-bonding partner of the main-chain carbonyl of position Thr 190. Being replaced by either the P1 Lys N^ε or Arg N^{η1} group thus maintains important hydrogen-bonding interactions within the S1 pocket. As with a P1 Arg bound in the S1 pocket, Sol 691 also is displaced when Lys binds (2KAI). Thus, the displaced solvent within the S1 pocket provides a “road map” for the locations of the side chain atoms of the P1 residue.

The width of the S1 binding pocket (quantified by the Cys 191 C α to Gly 216 C α distance) increases from 7.4 Å in human *apo* K1 to 7.9 Å in the porcine K1/hirustasin complex (1HIA–Arg in S1) or 8.1 Å in the porcine K1/BPTI complex (2KAI–Lys in S1). Thus, the S1 pocket expands its width by approximately 0.5–0.7 Å when the P1 residue is bound, presumably due to the larger *van der Waals* diameter of the P1 side-chain carbons. The water structure in the human *apo* K1 S1 pocket appears to be substantially different from that of the human K1 structure reported by Katz and coworkers.⁵⁰ Although five water molecules were identified within the S1 pocket by this group, they did not form a contiguous hydrogen-bonding network, and do not appear to be structurally equivalent to the water structure observed here.

S1' Pocket

The S1' pocket is defined by the side chains of residues Gln 41, Cys 42, His 57, and Cys 58 (with Cys 42 and Cys 58 forming a disulfide bond pair), and are identical between human and porcine K1 (Fig. 6). In the human *apo* K1 structure the S1' pocket is occupied by solvent molecules 854 and 789 that extend from the proximity of a bound P1' C^β outward, respectively. A comparison of the human *apo* K1 structure with that of porcine K1/benzamidine complex (2PKA; empty S1' pocket), porcine K1/BPTI complex (2KAI; with an Ala side chain occupying the S1' pocket) and porcine K1/Hirustasin complex (1HIA; with an Ile side chain occupying the S1' pocket) shows a consistent structural alteration depending on whether a peptide inhibitor is bound in the active site. In the absence of a bound peptide inhibitor (i.e., human *apo* K1 and porcine K1/benzamidine complex), the side chain of Gln 41 adopts a χ_2 angle of $\sim -60^\circ$. However, in the porcine K1/hirustasin and BPTI complexes the Gln 41 side chain adopts a χ_2 angle of $\sim 180^\circ$, “flipping up” and orienting lengthwise along the edge of the S1' pocket (Fig. 6). The rotation of the Gln 41 side chain appears necessary to avoid a steric clash with the main chain carbonyl oxygen of a bound P2' residue. Consequently the His 35 side chain must rotate out of the way of the repositioned Gln 41 side chain, and the His side chain rotates 120° , from the *gauche*+ rotamer to *trans* (i.e., in the porcine K1/BPTI and Hirustasin complexes; 2KAI and 1HIA, respectively). Inspection of the porcine K1/Hirustasin complex (1HIA) with an Ile side chain in the P1' position, shows that the side chain C^{γ1} and C^δ atoms follow the solvent 854 and 789 channel in human *apo* K1. Thus, a Lys side chain in the substrate P1' position is likely to adopt a *trans* rotamer and similarly

displace solvents 854 and 789 in the S1' pocket. The reoriented Gln 41 side chain would provide a *van der Waals* contact surface along the side of the S1' pocket for the aliphatic region of a bound P1' Lys side chain. The terminal N^ε group of the Lys chain would be positioned to hydrogen bond with both the main chain carbonyl of His 57 and the side chain N^{ε2} of the reoriented Gln 41 (potentially also Sol 657), displacing two solvent groups (854 and 789) in the process. Since the structural changes of Gln 41 appear to arise from the presence of a bound P2' main chain carbonyl, there is an apparent synergy between the binding of the P2' main chain and the P1' side chain, thus substrates lacking a P2' residue may exhibit reduced affinity for the P1' residue.

The dual substrate specificity of K1 includes cleavage of an Arg–Ser bond. A Ser side chain at the P1' position would be ideally juxtaposed to displace solvent 854 by the side chain O γ group, and hydrogen bond to solvent 789. Thus, the S1' pocket appears able to accommodate either a Lys or Ser side chain within the S1' pocket. In comparison to Lys, a Ser in the P1' position would displace a single solvent group. Since a Met in the S1 pocket would displace one to two fewer solvent than an Arg, the Met–Lys and Arg–Ser dual specificity of K1 is associated with similar solvent displacement effects in the S1 and S1' pockets.

S2' Pocket

The S2' pocket is a hydrophobic cleft formed by residue positions Phe 40, Phe 151, and Gly 193. These residues are identical between human and porcine K1 and are essentially juxtaposed when comparing an overlay of human *apo* K1 with either porcine K1/benzamidine complex (2PKA; empty S2' pocket), porcine K1/BPTI complex (2KAI; Arg in the P2' position), or porcine K1/hirustasin complex (1HIA; Arg in the P2' position). There are two solvent molecules located in the S2' pocket in human *apo* K1 (925 and 931) and these are displaced by the terminal guanidino group of the P2' Arg residue (figure not shown). Thus, other than the displacement of these solvent groups, there are no discernable structural changes in the S2' pocket upon substrate binding.

S2 to S2' Solvent Displacement by P2 to P2' Main-Chain Atoms

In addition to the previously described ordered solvent occupying the S2 to S2' pockets, there is a network of nine solvent molecules (616, 638, 651, 720, 726, 736, 741, 941, and 951) residing in positions occupied by the peptide main-chain atoms of the P2 to P2' residues in the porcine K1/inhibitor complexes. A tetrapeptide substrate or inhibitor bound within the S2 to S2' pockets can therefore potentially displace up to 18 ordered solvent molecules in the human K1 structure: nine displaced by the main-chain groups and up to nine displaced by the side chains (with the greatest single contribution being made by an Arg side chain in the S1 pocket). Related solvent networks, or “canals,” postulated to be displaced upon substrate binding, have been observed in high-resolution structures of bovine trypsin and porcine elastase,^{57,61} although neither

are as extensive as in hK1. The release of a localized solvent from a protein binding pocket is associated with an entropic gain of approximately 2.1 kcal/mol.⁶² Thus, the release of 18 solvent molecules in hK1 by a bound peptide inhibitor/substrate represents a substantial contribution to the overall binding free-energy.

CONCLUSION

In summary, the structure of human *apo* K1 contributes much-needed structural detail for a member of the human kallikrein family. When compared to the structures of porcine K1 with bound peptide inhibitors, the human *apo* K1 structure demonstrates a series of conformational changes in the active site, as well as S2 to S1' pockets, and provides a structural rationale for the accommodation of either Met or Arg residues in the S1 pocket, and Ser or Lys residues in the S1' pocket. The structural changes for Ser 195 in the active site, upon binding of peptides, are novel for a mature kallikrein and appear essential to achieve catalytic activity. The solvent hydrogen-bonding network in the active site, and S2 to S2' pockets, provides a "road map" for the positioning of bound peptide main-chain and side-chain groups within these sites, and results in the release of up to 18 water molecules with an associated entropic gain.

ACKNOWLEDGMENTS

We thank Ms. Margaret Seavy and Ms. Rani Dhanarajan in the Department of Biological Sciences at Florida State University for assistance with mass spectrometer data and generous cooperation in the baculovirus expression of human K1, respectively. X-ray structure coordinates have been deposited with the Protein Data Bank. This work was supported in part by grant RG3406-A-2 from the National Multiple Sclerosis Society, an American Heart Association Predoctoral fellowship 0315125B to G.L., and support from Fundação de Amparo a Pesquisa do Estado de São Paulo (FAPESP) to M.A.J.

REFERENCES

- Kraut H, Frey EK, Werle E. Der nachweis eines kreislaufhormon in der Pankreasdrüse. *Hoppe-Seyler's Zeitschrift für physiologische Chemie* 1930;189:97–106.
- Qin H, Kemp J, Yip M, Lam-Po-Tang PRL, Morris BJ. Localization of human glandular kallikrein-1 gene to chromosome 19q13.3-13.4 by *in-situ* hybridization. *Hum Hered* 1991;41:222–226.
- Riegman PH, Vlietstra RJ, Suurmeijer L, Cleutjens CB, Trapman J. Characterization of the human kallikrein locus. *Genomics* 1992;14:6–11.
- Yousef GM, Diamandis EP. The new human tissue kallikrein gene family: structure, function, and association to disease. *Endocr Rev* 2001;22:184–204.
- Olsson AY, Lundwall A. Organization and evolution of the glandular kallikrein locus in *Mus musculus*. *Biochem Biophys Res Commun* 2002;299:305–311.
- Oesterling JE. Prostate-specific antigen: a critical assessment of the most useful tumor marker for adenocarcinoma of the prostate. *J Urol* 1991;145:907–923.
- Catalona WJ, Smith DS, Ratliff TL, Dodds KM, Copley DE, Yuan JJ, Petros JA, Andriole GL. Measurement of prostate-specific antigen in serum as a screening test for prostate cancer. *New Engl J Med* 1991;324:1156–1161.
- Diamandis EP, Okui A, Mitsui S, Luo LY, Soosaipillai A, Grass L, Nakamura T, Howarth DJ, Yamaguchi N. Human kallikrein 11: a new biomarker of prostate and ovarian carcinoma. *Cancer Res* 2002;62:295–300.
- Yousef GM, Magklara A, Chang A, Jung K, Katsaros D, Diamandis EP. Cloning of a new member of the human kallikrein gene family, KLK14, which is down-regulated in different malignancies. *Cancer Res* 2001;61:3425–3431.
- Diamandis EP, Yousef GM, Petraki C, Soosaipillai AR. Human kallikrein 6 as a biomarker of Alzheimer's disease. *Clin Biochem* 2000;33:663–667.
- Diamandis EP, Yousef GM, Soosaipillai AR, Bunting P. Human kallikrein 6 (zyme/protease M/neurosin): a new serum biomarker of ovarian carcinoma. *Clin Biochem* 2000;33:579–583.
- Luo LY, Bunting P, Scorilas A, Diamandis EP. Human kallikrein 10: a novel tumor marker for ovarian carcinoma? *Clin Chim Acta* 2001;306:111–118.
- Yamanaka H, He X, Matsumoto K, Shiosaka S, Yoshida S. Protease M/neurosin mRNA is expressed in mature oligodendrocytes. *Brain Res Mol Brain Res* 1999;71:217–224.
- Scarlsbrick IA, Asakura K, Blaber S, Blaber M, Isackson PJ, Bieto T, Rodriguez M, Windebank AJ. Preferential expression of myelencephalon-specific protease by oligodendrocytes of the adult rat spinal cord white matter. *Glia* 2000;30:219–230.
- Scarlsbrick IA, Isackson PJ, Ciric B, Windebank AJ, Rodriguez M. MSP, a trypsin-like serine protease, is abundantly expressed in the human nervous system. *J Comp Neurol* 2001;431:347–61.
- Scarlsbrick IA, Towner MD, Isackson PJ. Nervous system-specific expression of a novel serine protease: regulation in the adult rat spinal cord by excitotoxic injury. *J Neurosci* 1997;17:8156–8168.
- Blaber SI, Scarlsbrick IA, Bernett MJ, Dhanarajan P, Seavy MA, Jin Y, Schwartz MA, Rodriguez M, Blaber M. Enzymatic properties of rat myelencephalon specific protease. *Biochemistry* 2002;41:1165–1173.
- Ogawa K, Yamada T, Tsujioka Y, Taguchi J, Takahashi M, Tsuboi Y, Fujino Y, Nakajima M, Yamamoto T, Akatsu H and others. Localization of a novel type trypsin-like serine protease, neurosin, in brain tissues of Alzheimer's disease and Parkinson's disease. *Psychiatry Clin Neurosci* 2000;54:419–426.
- Kishi T, Kato M, Shimizu T, Kato K, Matsumoto K, Yoshida S, Shiosaka S, Hakoshima T. Crystallization and preliminary X-ray analysis of neuropsin, a serine protease expressed in the limbic system of mouse brain. *J Struct Biol* 1997;118:248–251.
- Kishi T, Kato M, Shimizu T, Kato K, Matsumoto K, Yoshida S, Shiosaka S, Hakoshima T. Crystal structure of neuropsin, a hippocampal protease involved in kindling epileptogenesis. *J Biol Chem* 1999;274:4220–4224.
- Silva J-A, Jr., Araujo RC, Baltatu O, Oliveira SM, Tschope C, Fink E, Hoffmann S, Plehm R, Chai KX, Chao J and others. Reduced cardiac hypertrophy and altered blood pressure control in transgenic rats with the human tissue kallikrein gene. *FASEB J* 2000;14:1858–1860.
- Fiedler F, Leysath G. Substrate specificity of porcine pancreatic kallikrein. *Adv Exp Med Biol* 1979;120A:261–271.
- Clements JA. The molecular biology of the kallikreins and their roles in inflammation. In: Farmer SG, editor. *The Kinin system*. Volume 5. San Diego: Academic Press; 1997. p 71–97.
- Margolius HS. Kallikreins, kinins and cardiovascular diseases: a short review. *Biol Res* 1998;31:135–141.
- Margolius HS. Tissue kallikreins structure, regulation, and participation in mammalian physiology and disease. *Clin Rev Allergy Immunol* 1998;16:337–349.
- Crackower MA, Sarao R, Oudit GY, Yagil C, Kozieradzki I, Scanga SE, Oliveira-dos-Santos AJ, da Costa J, Zhang L, Pei Y and others. Angiotensin-converting enzyme 2 is an essential regulator of heart function. *Nature* 2002;417:822–828.
- Erdos EG. Conversion of angiotensin I to angiotensin II. *Am J Med* 1976;60:749–759.
- Bode W, Chen Z, Bartels K, Kutzbach C, Schmidt-Kastner G, Bartunik H. Refined 2 Å X-ray crystal structure of porcine pancreatic kallikrein A, a specific trypsin-like serine proteinase. Crystallization, structure determination, crystallographic refinement, structure and its comparison with bovine trypsin. *J Mol Biol* 1983;164:237–282.
- Chen Z, Bode W. Refined 2.5 Å X-ray crystal structure of the complex formed by porcine kallikrein A and the bovine pancreatic trypsin inhibitor. Crystallization, Patterson search, structure determination, refinement, structure and comparison with its

- components and with the bovine trypsin-pancreatic trypsin inhibitor complex. *J Mol Biol* 1983;164:283–311.
30. Mittl PR, Di Marco S, Fendrich G, Pohlig G, Hein J, Sommerhoff C, Fritz H, Priestel JP, Grutter MG. A new structural class of serine protease inhibitors revealed by the structure of the hirustasin-kallikrein complex. *Structure* 1997;5:253–264.
 31. Carvalho AL, Sanz L, Baretino D, Romero A, Calvete JJ, Romao MJ. Crystal structure of a prostate kallikrein isolated from stallion seminal plasma: a homologue of human PSA. *J Mol Biol* 2002;322:325–337.
 32. Bax B, Blundell TL, Murray-Rust J, McDonald NQ. Structure of mouse 7S NGF: a complex of nerve growth factor with four binding proteins. *Structure* 1997;5:1275–1285.
 33. Timm DE. The crystal structure of the mouse glandular kallikrein-13 (prorenin converting enzyme). *Protein Sci* 1997;6:1418–1425.
 34. Fujinaga M, James MN. Rat submaxillary gland serine protease, tonin. Structure solution and refinement at 1.8 Å resolution. *J Mol Biol* 1987;195:373–396.
 35. Bernett MJ, Blaber SI, Scarisbrick IA, Dhanarajan P, Thompson SM, Blaber M. Crystal structure and biochemical characterization of human kallikrein 6 reveals a trypsin-like kallikrein is expressed in the central nervous system. *J Biol Chem* 2002;277:24562–24570.
 36. Gomis-Ruth FX, Bayes A, Sotiropoulou G, Pampalakis G, Tsetsenis T, Villegas V, Aviles FX, Coll M. The structure of human prokallikrein 6 reveals a novel activation mechanism for the kallikrein family. *J Biol Chem* 2002;277:27273–27281.
 37. Gill SC, von Hippel PH. Calculation of protein extinction coefficients from amino acid sequence data. *Anal Biochem* 1989;182:319–326.
 38. Jancarik J, Kim S-H. Sparse matrix sampling: a screening method for crystallization of proteins. *J Appl Crystallogr* 1991;24:409–411.
 39. Otwinowski Z. Oscillation data reduction program. In: Sawyer L, Isaacs N, Bailey S, editors; 1993, Jan 29–30. SERC Daresbury Laboratory, England. p 56–62.
 40. Otwinowski Z, Minor W. Processing of x-ray diffraction data collected in oscillation mode. *Meth Enzymol* 1997;276:307–326.
 41. Brunger AT, Adams PD, Clore GM, DeLano WL, Gros P, Grosse-Kunstleve RW, Jiang JS, Kuszewski J, Nilges M, Pannu NS and others. Crystallography & NMR system: A new software suite for macromolecular structure determination. *Acta Crystallogr D Biol Crystallogr* 1998;54:905–921.
 42. Brunger AT. Free *R* value: a novel statistical quantity for assessing the accuracy of crystal structures. *Nature* 1992;355:472–475.
 43. Jones TA, Zou JY, Cowan SW, Kjeldgaard M. Improved methods for the building of protein models in electron density maps and the location of errors in these models. *Acta Crystallographica* 1991;A47:110–119.
 44. Guex N, Peitsch MC. SWISS-MODEL and the Swiss-Pdb Viewer: An environment for comparative protein modeling. *Electrophoresis* 1997;18:2714–2723.
 45. Shimamoto K, Chao J, Margolius HS. The radioimmunoassay of human urinary kallikrein and comparisons with kallikrein activity measurements. *J Endocrinol Metabol* 1980;51:840–859.
 46. Sampaio CA, Sampaio MU, Prado ES. Active-site titration of horse urinary kallikrein. *Hoppe-Seyler's Zeitschrift fur physiologische Chemie* 1984;365:297–302.
 47. Hirata IY, Cezari MHS, Nakaie C, Boschov P, Ito AS, Juliano M, Juliano L. Internally quenched fluorogenic protease substrates: Solid-phase synthesis and fluorescence spectroscopy of peptides containing *ortho*-aminobenzoyl/dinitrophenyl groups as donor-acceptor pairs. *Lett Pept Sci* 1994;1:299–308.
 48. Wilkinson GN. Statistical estimations in enzyme kinetics. *Biochem J* 1961;80:324–332.
 49. Matthews BW. Solvent content of protein crystals. *J Mol Biol* 1968;33:491–497.
 50. Katz BA, Beishan L, Barnes M, Springman EB. Crystal structure of recombinant human tissue kallikrein at 2.0 Å resolution. *Protein Sci* 1998;7:875–885.
 51. Villoutreix BO, Getzoff ED, Griffin JH. A structural model for the prostate disease marker, human prostate-specific antigen. *Protein Sci* 1994;3:2033–2044.
 52. Matthews BW, Sigler PB, Henderson R, Blow DM. Three-dimensional structure of tosyl- α -chymotrypsin. *Nature* 1967;214:652–656.
 53. Birktoft JJ, Blow DM. Structure of crystalline chymotrypsin. V. The atomic structure of tosyl-chymotrypsin at 2 Å resolution. *J Mol Biol* 1972;68:187–240.
 54. Freer ST, Kraut J, Robertus JD, Wright HT, Xuong NG. Chymotrypsinogen: 2.50-Å crystal structure, comparison with α -chymotrypsin, and implications for zymogen activation. *Biochemistry* 1970;9:1997–2009.
 55. Kossiakoff AA, Chambers JL, Kay LM, Stroud RM. Structure of bovine trypsinogen at 1.9 Å resolution. *Biochemistry* 1977;16:654–664.
 56. Bode W, Schwager P. The refined crystal structure of bovine β -trypsin at 1.8 Å resolution. *J Mol Biol* 1975;98:693–717.
 57. Bartunik HD, Summers LJ, Bartsch HH. Crystal structure of bovine b-trypsin at 1.5 Å resolution in a crystal form with low molecular packing density. *J Mol Biol* 1989;210:813–828.
 58. Deshpande MS, Burton J. Mapping the binding site of tissue kallikrein: preparation and testing of all possible substrate analog inhibitors homologous with the sequence of kininogen between Ser386 and Gln392. *J Med Chem* 1992;35:3094–3102.
 59. Chagas JR, Portaro FC, Hirata IY, Almeida PC, Juliano MA, Juliano L, Prado ES. Determinants of the unusual cleavage specificity of lysyl-bradykinin-releasing kallikreins. *Biochem J* 1995;306:63–69.
 60. Helland R, Otlewski J, Sundheim O, Dadlez M, Smalas AO. The crystal structures of the complexes between bovine β -trypsin and ten P1 variants of BPTI. 1999;284:923–942.
 61. Meyer E, Cole G, Radhakrishnan R, Epp O. Structure of native porcine pancreatic elastase at 1.65 Å resolution. *Acta Crystallogr B* 1988;44:26–38.
 62. Hamelberg D, McCammon JA. Standard free energy of releasing a localized water molecule from the binding pockets of proteins: double-decoupling method. *J Am Chem Soc* 2004;126:7683–7689.